NUMERICAL REPRODUCTION OF EXPERIMENTAL ICE COVER MELTING

by
R. Saadé
Tecsult Inc.
Department of Geotechnical and Hydraulic Resources
85 Rue St. Catherine Montreal,
Quebec, H2X 3P4
and
S.Sarraf
Concordia University
Associate Professor Civil Engineering Department,
1455 de Maisonneuve Blvd.W., Montreal,
Qc, Canada, H3G 1M8

ABSTRACT

Ice cover is formed on rivers in cold regions for most of the winter season. This effects the usage of these rivers for transportation, power generation, water supply and municipal and industrial waste water disposal. For an ice cover in contact with air at or below the freezing point of water, and with sufficiently warm flow of water beneath the ice cover, melting occurs at the water-ice interface. However, there is an increase rate in melting at the leading edge of the ice cover and a decrease in the melting rate in the downstream direction.

A two-dimensional turbulence model for the simulation of river hydrodynamics under ice cover conditions and the melting of the ice cover due to warm water is presented. The velocity field is obtained from the St. Venant equations; the unsteady two-dimensional energy equation is used to obtain the temperature field; and the k-e model was used to evaluate the turbulent characteristics of the flow. The change in the ice thickness was obtained from the use of heat transfer equations which occur at the water-ice interface and ice-air interface.

The upwind finite-difference scheme was applied to the transport equations, and a modified version of the MacCormack scheme is used to solve for the hydrodynamic equations.

Three sets of laboratory studies were numerically reproduced using the model. The ice cover melting under turbulent flow conditions was investigated.

KEY WORDS: Turbulence, ice cover, numerical modelling, melting, k-epsilon, thermal, effluent, simulation.

INTRODUCTION

During the cold season in northern countries, the occurrence of ice covers on rivers and channels attributes to problems related to transportation, power generation, water supply, municipal and industrial wastewater disposal and flood control. Of major concern to hydraulics engineers is the development of methods to prevent or at least to control the formation of ice covers.

Few investigations have been carried out on heat transfer problems of river ice. Methods to predict ice formation on rivers have been developed based on the analysis of meteorological and river flow records. Bilello(1963) had made an attempt to adapt this relationship to predict river and lake ice formation under specified meteorological and stream flow conditions. None of the methods that estimate the length of ice free reaches have dealt with the decay of ice. In these studies, it has been assumed that ice cover formation occurs only when the river temperature reaches the freezing point. Field observations have long shown that under cold weather conditions, an ice cover can form even when the river ambient temperature is several tenths of a degree above 0 °C depending on air temperatures, wind and other meteorological conditions.

Hewlett (1976), investigated the rate of melting of an ice cover due the addition of a heat source. Shen and Chiang 1984, developed a one-dimensional model of the ice cover growth and decay on the St. Lawrence River using a uniform velocity field and including a complete ice cover and open water heat transfer formulation.

The present paper is focused mainly on the influence of warm water on the change in the ice cover thickness under turbulent flow conditions. Emphasis is made on the extent of the change in ice cover thickness as a function of time.

GOVERNING EQUATIONS

Flows dominated by a negligible hydraulic gradient and a small depth to width ratio, the flow regime in rivers can be conveniently described by the depth-averaged equations of motion. This is true in the case of transport of temperature where the depth averaged heat equation can be used. Hewlett 1976, noted that there was negligible temperature variation along the depth while performing their laboratory work. Also, the negligible variation in the water temperature under an ice cover is supported by field observation taken by Ashton 1979 at the Mississippi River, and March and Prowse 1986 at the Liard River.

The depth-averaged continuity, momentum, k, ε and temperature equations, used by the model, in conservative form are expressed in vector form as follows:

$$[1] \qquad \frac{\partial \psi(t)}{\partial t} + \frac{\partial \psi(x)}{\partial x} + \frac{\partial \psi(y)}{\partial y} = F$$

where

$$[2] \qquad \psi(t) = \begin{bmatrix} H \\ uh \\ vh \\ kh \\ \varepsilon h \\ Th \end{bmatrix}; \psi(x) = \begin{bmatrix} uh \\ u^2h - \frac{\tau_{xx}}{\rho} + PZ_T \\ uvh - \frac{\tau_{xy}}{\rho} \\ ukh - \frac{\nu_t h}{\sigma_k}\frac{\partial k}{\partial x} \\ u\varepsilon h - \frac{\nu_t h}{\sigma_\varepsilon}\frac{\partial \varepsilon}{\partial x} \\ uTh - \Gamma_T h \frac{\partial T}{\partial x} \end{bmatrix}; \psi(y) = \begin{bmatrix} vh \\ uvh - \frac{\tau_{yx}}{\rho} \\ v^2h + PZ_T - \frac{\tau_{yy}}{\rho} \\ vkh - \frac{\nu_t h}{\sigma_k}\frac{\partial k}{\partial y} \\ v\varepsilon h - \frac{\nu_t h}{\sigma_\varepsilon}\frac{\partial \varepsilon}{\partial y} \\ vTh - \Gamma_T h \frac{\partial T}{\partial y} \end{bmatrix}; F = \begin{bmatrix} 0 \\ \frac{\tau_{sx}}{\rho} - \frac{\tau_{bx}}{\rho} \\ \frac{\tau_{sy}}{\rho} - \frac{\tau_{by}}{\rho} \\ G + P_{kv} - \varepsilon h \\ C_1\frac{\varepsilon}{k}G + P_{\varepsilon v} - C_2\frac{\varepsilon^2 h}{k} \\ \phi \end{bmatrix}$$

in which $Z_T = [h + Z_o + 0.92(\theta)]$; $P = gh/2$; θ = ice cover thickness; τ_{sx}, τ_{sy} = surface stresses; uh, vh = unit discharges in the x and y directions respectively; τ_{bx}, and τ_{by} = bottom shear stresses per unit mass in the x and y directions respectively expressed as follows:

$$[3] \qquad \frac{\tau_{bx}}{\rho} = g\,h\,(S_{ox} - S_{fx}) \qquad [5] \qquad S_{fx} = \frac{n^2 u q}{R^{4/3}}$$

$$[4] \qquad \frac{\tau_{by}}{\rho} = g\,h\,(S_{oy} - S_{fy}) \qquad [6] \qquad S_{fy} = \frac{n^2 v q}{R^{4/3}}$$

S_{ox}, S_{oy} = river bed slopes, $q = C_f (u^2 + v^2)^{1/2}$,

and the combined Manning coefficient is obtained form the following formula:

$$[7] \qquad n = \left(\frac{n_b^{3/2} + n_i^{3/2}}{2} \right)^{2/3}$$

C_f = drag coefficient for water flowing over a fixed surface, R = hydraulic radius; n = Manning's surface roughness coefficient; n_b is the bed roughness coefficient and n_i is the ice underside roughness coefficient.

The temperature distribution in the flow field is computed using the heat equation . The turbulent diffusion heat flux coefficient Γ_T contained in the heat equation is determined over the flow domain by the following relation:

[8] $$\Gamma_T = \frac{\nu_t}{\sigma_T}$$

where σ_T is 0.9, and ν_t is the turbulent viscosity. The k-ε turbulence model chatacterizes the local state of turbulence by the turbulent kinetic energy k that originates from the turbulent flow, and the rate of its dissipation ε.The turbulent diffusion coefficient contained in the k and ε equations are evaluated over the flow domain by the folowing relations, respectively:

[9] $$\Gamma_k = \frac{\nu_t\, h}{\sigma_k}$$ [10] $$\Gamma_\varepsilon = \frac{\nu_t\, h}{\sigma_\varepsilon}$$

and the source terms found in the k and ε equations are evaluated as follows respectively:

[11] $\Phi_k = G + P_{kv} - \varepsilon h$ [12] $\Phi_\varepsilon = C_1\,(\varepsilon/k)\,G + P_{\varepsilon v} - C_2\,(\varepsilon^2 h/k)$

where

[13] $$G = \frac{\nu_t}{h}\left[\, 2\left(\frac{\partial uh}{\partial x}\right)^2 + 2\left(\frac{\partial vh}{\partial y}\right)^2 + \left(\frac{\partial uh}{\partial y} + \frac{\partial vh}{\partial x}\right)^2 \right]$$

represents the production of turbulent kinetic energy in the horizontal direction due to interactions of turbulent stresses with horizontal mean velocity gradients; and the empirical constants $\sigma_k = 1.0$, $C_1 = 1.43$, and $C_2 = 1.92$. In addition to the turbulent production G, bottom roughness contributes significantly to vertical velocity gradients, which by interaction with large turbulent shear stresses, produce turbulence energy in the vertical direction which is absorbed in the P_{kv} and $P_{\varepsilon v}$ terms, which are expressed as follows:

[14] $$P_{kv} = \frac{C_f}{h}\, q^4$$

[15] $$P_{\varepsilon v} = \frac{C_2\, C_\mu\, C_f^{5/4}}{h^2}$$

where

[16] $$q = \sqrt{(u^2 + v^2)}$$

The method used to calculate the shear stress terms in the momentum equations is based on the eddy viscosity concept which is represented by the following expression: Using tensor notations (McGuirk and Rodi 1978)

$$[17] \quad \frac{\tau_{ij}}{\rho} = \nu_t h \left(\frac{\partial u_i}{\partial x_j} + \frac{\partial u_j}{\partial x_i} \right) - \frac{2}{3} k h \delta_{ij}$$

where ν_t represents the eddy viscosity given by the following expression:

$$[18] \quad \nu_t = C_\mu \frac{k^2}{\varepsilon}$$

where C_μ is an empirical constant.

GROWTH AND DECAY OF A SOLID ICE COVER

Heat transfer processes on the surface of a river occurs across the water-air interface, ice-air interface, and water-ice interface as shown in figure 1. The heat fluxes across the ice-air interface is greatly affected by the fluctuation of air temperature, while, the heat flux at the water-ice interface depends mainly on the river flow conditions with the interface temperature assumed at the freezing point 0°C. The heat transfer at the ice-air interface is governed by the solar radiation components.

Heat fluxes at the top surface of the ice cover are dependent on the prevailing meteorological conditions. The melting at the top surface of the ice cover is expressed as follows:

$$[19] \quad \phi_m + K_i \frac{T_f - T_s}{\theta} = - \rho_i L_i \frac{d\theta}{dt}$$

where ϕ_m is the net heat loss rate at the air-ice interface; L_i is the latent heat of fusion of ice, 8 x 10^4 cal./Kg; ρ_i is the density of ice which, 920 Kg/m^3; and θ is the ice cover thickness in meters. ϕ_m is the sum of the heat exchange components, the net solar radiation (ϕ_s), the penetrating shortwave radiation (ϕ_{sp}), the longwave radiation (ϕ_b), the evapo-condensation heat flux (ϕ_e), and the conductive heat transfer (ϕ_c), expressed by the following expression:

$$[20] \quad \phi_m = \phi_s - \phi_{sp} - \phi_b - \phi_e - \phi_c$$

The melting and thickening of the ice cover at the water-ice interface is governed by the energy balance at the water-ice interface expressed as follows:

$$[21] \quad K_i \frac{T_f - T_s}{\theta} - \phi_{wi} = \rho_i L_i \frac{\Delta\theta}{\Delta t}$$

the heat flux from the water to the ice cover is

[22] $\phi_{wi} = h_{wi} (T_w - T_f)$ such that

[23] $h_{wi} = C_{wi} \frac{U^{0.8}}{D^{0.2}}$

is a heat transfer coefficient such that U is the average water velocity in m/s; C_{wi} equals 1622 W $S^{0.8}m^{-2.6}C^{-1}$; D is the flow depth in meters; ρ_i is the density of ice in Kg m^{-3}; L_i is the heat of fusion in j Kg^{-1} and $\Delta\theta/\Delta t$ is the rate of change of the thickness of the ice.

The heat source in the heat equation is evaluated from the combination of the heat flux components. Recall, the heat source term is given by the following formula:

[24] $\Phi = \frac{\Sigma\phi}{C_p \rho}$

where C_p is the specific heat capacity; h is the depth of flow; and ρ is the water density; and $\Sigma\phi$ is the sum of related heat fluxes expressed as follows: (Ashton 1978, & Shen and Chiang 1984)

[25] $\Sigma\phi = \phi_{sp} - \phi_{wi}$ for ice covered river

[26] $\Sigma\phi = \phi_s - \phi_b - \phi_e - \phi_c - \phi_{wa}$ for open channels

NUMERICAL COMPUTATION

The MacCormack Scheme

The solution of the depth-averaged St. Venant equations is obtained by applying an explicit finite difference method based on the modified MacCormack time splitting scheme (Garcia et. al., 1983). The scheme is forward time, central space, which involves the splitting of a two-dimensional calculation into a sequence of two one-dimensional operations such that, each operator is further split into a predictor-corrector sequence as follows:

First	L_x *operator*	*Predictor:*	*Backward Difference*
		Corrector:	*Forward Difference*
First	L_y *operator*	*Predictor:*	*Backward Difference*
		Corrector:	*Forward Difference*
Second	L'_y *operator*	*Predictor:*	*Forward Difference*
		Corrector:	*Backward Difference*
Second	L'_x *operator*	*Predictor*	*Forward Difference*
		Corrector:	*Backward Difference*

where L_x and L_y are the one dimensional finite-difference operators. The L_x and L_y operators calculate the derivatives in the x and y directions respectively.The step that follows the predictor-corrector sequence is the averaging of the value obtained

from the previous two steps. The stability conditions are determined by the Courent-Freidrich-Levy criterion which states that the maximum time step that can be used in the standard MacCormack scheme is the minimum value of the following two terms:

$$[27] \quad \Delta T = \text{MIN.}\left[\frac{\Delta X}{u + \sqrt{g\,h}}, \frac{\Delta Y}{v + \sqrt{g\,h}}\right]$$

The Upwind Scheme

The use of an upwind scheme is suitable when steady or near steady convection is dominate in the development of the temperature field and either the flow is closely aligned with the grid lines or no strong cross flow gradients are present [Raithby 1976]. The upwind scheme is an explicit forward time method which takes into account the direction of the convecting velocity such that it is used as a remedy to the difficulties and weaknesses found in the formulation of the other numerical schemes. The scheme used for the solution of the diffusion terms in the transport equations is left unchanged, however the value of the convective property assumes the value of the same property of the grid point on the upwind side of the face as follows (Patankar 1980):

BOUNDARY CONDITIONS

At the upstream inlet boundary the velocity and temperature are specified, and at the downstream outlet boundary the water depth is specified.

The dissipation of turbulent kinetic energy ε in the near-wall region and the shear stess τ_w at the solid surface are determined as follows:

$$[28] \quad \varepsilon = \frac{U_*^3}{\kappa\, y_w}$$

$$[29] \quad \frac{\tau_\omega}{\rho} = \frac{U_* \kappa\, U_w}{\ln\left(\frac{y_0}{Z_0}\right)^2}$$

where k_w, ε_w = turbulent kinetic energy and rate of dissipation respectively in the near-wall region; U_w = resultant velocity parallel to the wall; U_* = resultant friction velocity; κ = von karman constant; $\Delta y/2$ = half the grid spacing; and Z_o = channel roughness height; y_w is the distance from the wall to the center of the nearest cell (half the grid spacing).

The velocity U_w and the turbulent kinetic energy k_w, in the wall region, are calculated from their corressponding balance equations such that the modification to ε is to account for the large increase in dissipation rate in the near-wall region, where the ε expression used in the k equation is given by:

[30] $$\varepsilon = \frac{U_*^3}{\kappa y_w} \ln\left(\frac{\Delta y}{Z_0}\right)$$

The normal gradient of u, v and k at the wall are set to zero. The temperature gradients are also zero since negligible heat transfer through the wall is assumed in most hydraulic problems. The walls are assumed to be adiabatic walls, where the heat and concentration flux are taken as zero, and the normal gradient of the water level, ice cover thickness, bottom elevation and hydraulic radius were set to zero at the cell adjacent to the wall.

MODEL APPLICATION

Experimental Set-up

In this study a turbulence model is used to predict the melting rate of an ice cover subjected to water at above zero temperature, and air at or below zero temperature. Three experiments that were performed by Hewlett 1974 were reproduced numerically. Hewlett made an attempt to analyze the rate and pattern of melting near the upstream end of an ice slab floating on turbulent flowing water.

A 5 cm. initial ice cover thickness was produced over an approximate water depth of 20 cm. The channel inlet extended downstream 210 cm free surface, 820 cm. ice-covered and 170 cm free surface at the outlet section, with a constant width of 60 cm. The inlet temperature is assumed to maintain a mean value of 1°C after time t = 0. The air temperature is set to 0°C such that the net heat flux to the ice cover is positive (upward). The mean discharge per unit width was kept at a constant mean value of q =2.23 m^2/minutes.

Numerical Reproduction

Three experiments were numerically duplicated. The geometry of the channel was first fitted into a uniform grid system where the cell size is 0.2m by 0.03m, then initial conditions were imposed. The velocity field was set to a constant value of 0.186 m sec^{-1} and the temperature distribution over the entire domain was initialized to 1°C. The air temperature was set to 0°C; the wind velocity was set to approximately 20KPH under the assumption of such a wind in the lab

would be due to the cooling system; and the cloud cover was set to 90% clouds.

After that steady-state was achieved, the ice cover was introduced with the exact thicknesses as measured in the laboratory, and the water depth upstream was increased from 0.2 m to 0.246m.

RESULTS / DISCUSSION

Figures 2, 3, and 4 present a comparison of the longitudinal ice cover thickness profiles between computed and measured data for 3 experiments say 1, 2, and 3 respectively, at 100, 200, and 300 minutes. The difference between measured and computed ice cover melting pattern is identified in two regions. The first region is located near the leading edge of the ice cover, while the second region extends over the rest of the downstream portion of the ice cover. In the leading edge region, experiment 1 reveals that the predicted longitudinal ice cover thickness profile after 100 min of the commencement of the melting process compares very favorably to the measured longitudinal ice cover thickness profile. However, beyond 100 min, the difference in the rate of change between predicted and measured ice cover thicknesses increase, at times 200 min and 300 min, with predicted ice cover thicknesses less than measured ice cover thicknesses.

However, the difference between the measured and computed ice cover thickness profiles found in experiment 3 is small, as shown in figure 3, and the melting pattern of the ice cover is simulated with very good accuracy in both the leading edge as well as at the downstream region of the ice cover. Experiment 2 on the other hand, results in a relatively unsatisfactory difference between measured and computed ice cover thickness profiles, as shown in figure 4. The ice cover melting extent is underpredicted over the entire ice cover domain.

In spite of the complex, unsteady hydrodynamics and thermal conditions in the experimental tests near the leading edge, and the oscillatory behavior of the rate of ice cover melting in the leading edge region, it was found and confirmed numerically that after a certain distance from the leading edge, the ice cover melting as a function of time can be approximated by a straight line. The measured and predicted ice cover thicknesses are compared in figure 5 for experiment 1, 6 for experiment 2, and 7 for experiment 3.

Straight lines represent the difference between measured and predicted ice cover thicknesses. Scattered data represent non-linear behavior, and lines with a steep slope indicate larger error between measured and predicted data, such as the case in the leading edge region. A curve below the zero level indicates

that the predicted rate of melting is larger than the measured rate of melting.

The total amount of melting of the ice cover is predicted with very good accuracy. The average melting of the ice cover is represented in figures 8 to 10, for experiments 1, 3, and 2 respectively. The predicted average ice cover thicknesses for experiments 1 and 6 are in very good agreement with the measured ice cover thicknesses. However, for experiment 2, the computed average ice cover thicknesses are greater than the measured ones, due to the underprediction of the ice cover thicknesses throughout the ice cover.

The predicted melting of the ice cover edge approximate sufficiently well the measured values for the first 150 min of computations. Thereafter, the numerical prediction for the edge melting were underestimated compared to actual observations. In fact, the theory of heat transfer from water to ice applied does not take into effect the turbulent behavior of water acceleration at the ice cover edge. A study was performed by Wang, Y., "Report of Ice Melting Experiment and Calculation", Internal Report, Concordia University, Nov. 1989, to test the effects of three different methods of heat transfer at the water-ice interface and compare them to experimental data. The heat transfer coefficient calculations used in determining the melting of the ice cover are based on a constant temperature at infinity, variable temperature at infinity, laminar boundary layer, and turbulent flow. The effect of a variable temperature assumption on the results were small and therefore neglected.

CONCLUSION

A two-dimensional turbulence model for the melting of the ice cover due to warm water and under turbulent flow conditions was used to numerically reproduce three experimental ice cover melting studies. The model computes velocity field from the St. Venant equations; the temperature distribution from the unsteady two-dimensional energy equation; and the k-ε model for the turbulent characteristics of the flow. The change in the ice thickness was obtained from the use of heat transfer equations which occur at the water-ice interface and ice-air interface.

Results have shown that the melting of an ice cover due to warm water is computed with a good accuracy. However, discrepancies do exist in which they can be attributed to the method of formation of the ice cover in the lab, the heat transfer coefficient at the water-ice interface, the variability in the inlet temperature and discharge and the boundary conditions at the ice cover interfaces.

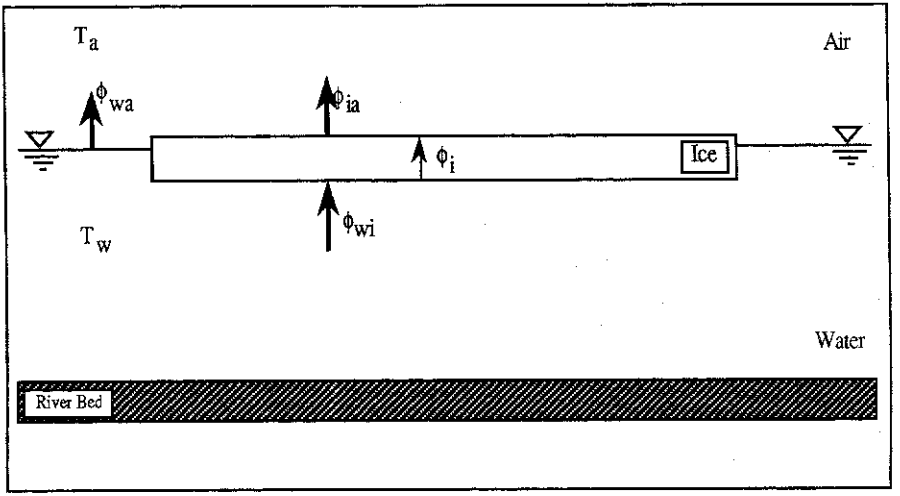

Figure 1. Heat Transfer at The River Surface.

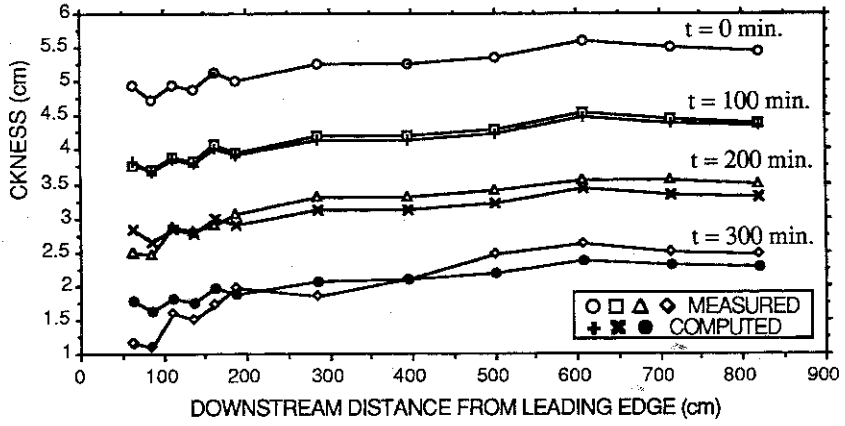

Figure 2. Longitudinal Ice Cover Thickness Profiles for Experiment #1.

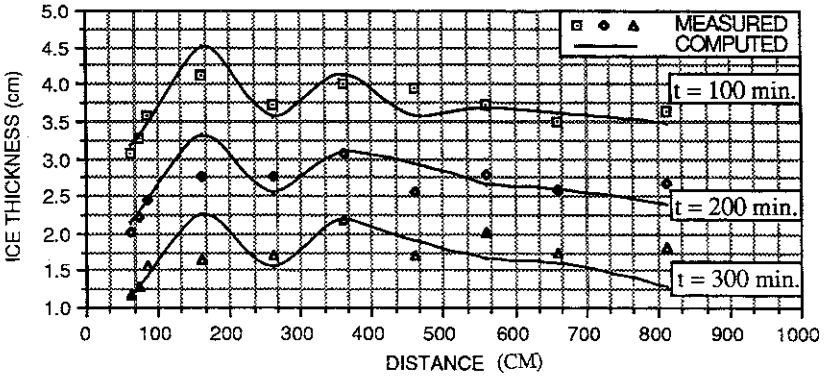

Figure 3. Longitudinal Ice Cover Thickness Profiles for Experiment #3.

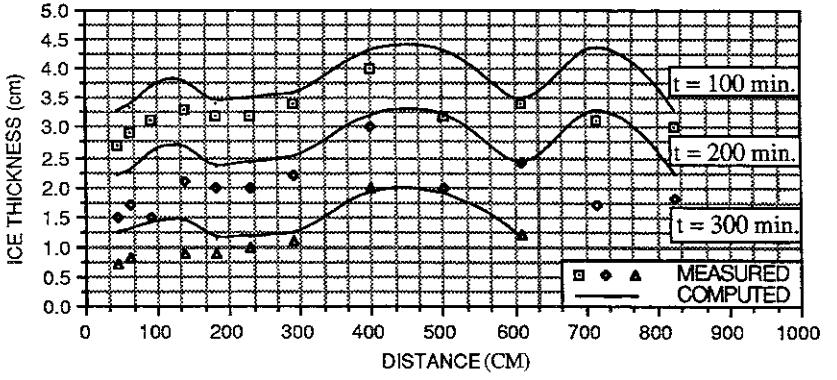

Figure 4. Longitudinal Ice Cover Thickness Profiles for Experiment #2.

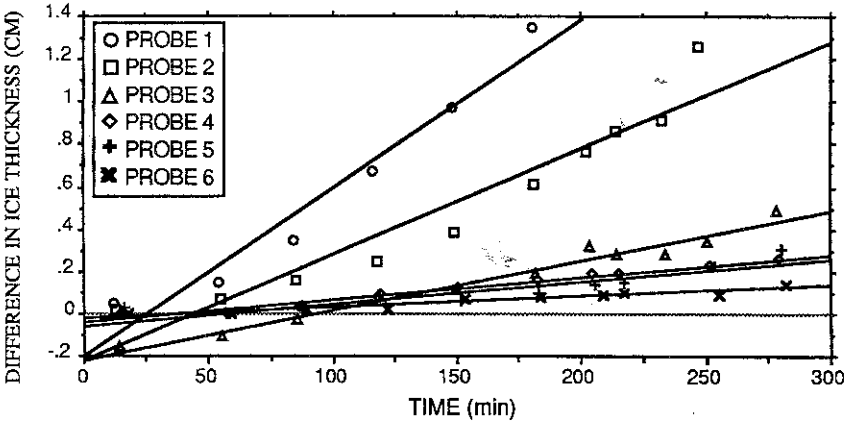

Figure 5. Difference in Ice Cover Thickness for Exp. # 1.

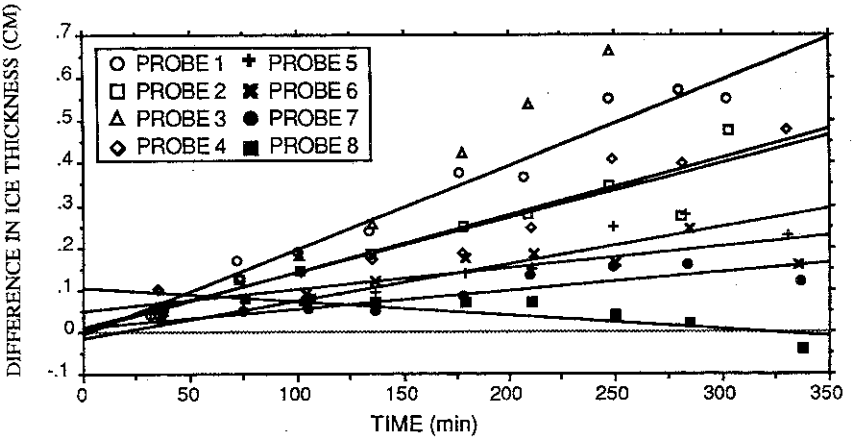

Figure 6. Difference in Ice-Cover Thickness at Probe Locations in Exp. 2.

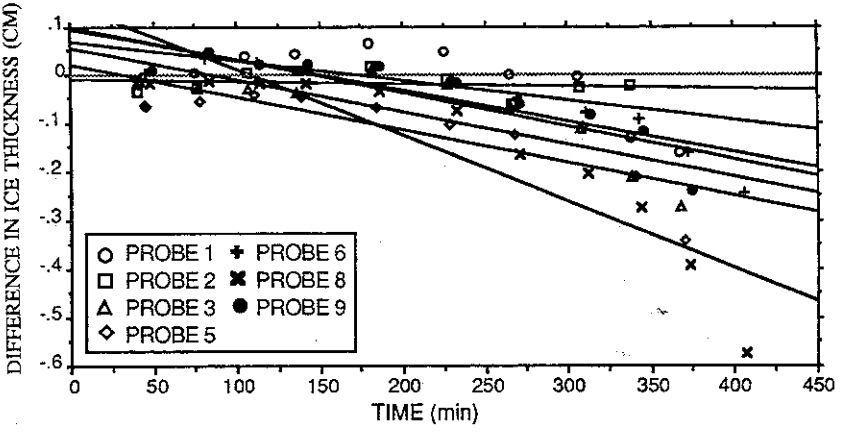

Figure 7. Difference in Ice-Cover Thickness for Exp. 3.

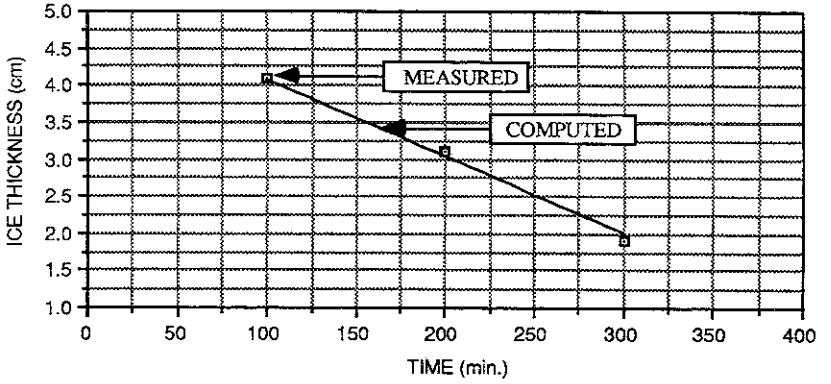

Figure 8. Average ice cover thickness for experiment #1.

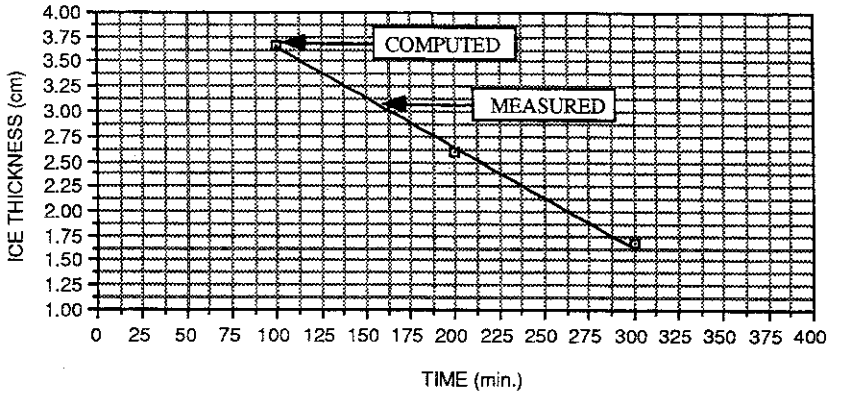

Figure 9. Average ice cover thickness for experiment #3.

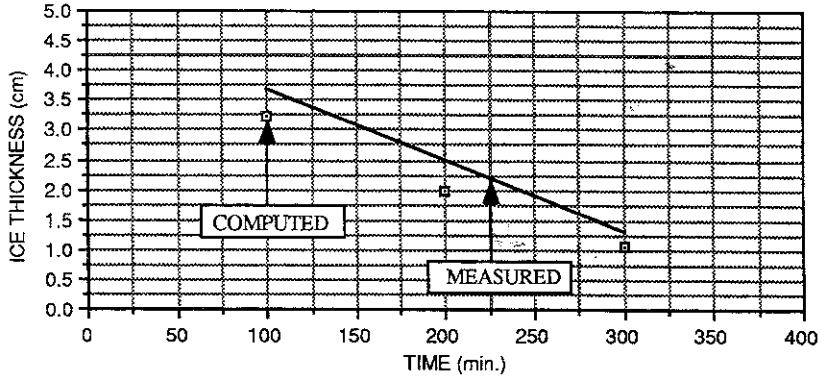

Figure 10. Average ice cover thickness for experiment #2.

REFERENCES

1. Ashton, G.D. (1979), "Suppression of River Ice by Thermal Effluents", U.S. Army Cold Regions Research Engineering Laboratory, CRREL Report 79-30, Hanover, N.H., Dec.
2. Chapman, S.R. (1982), "A numerical simulation of two-dimensional separated flow in a symmetric open-channel expansion using the depth integrated two-equation (K-Epsilon) turbulence closure model", Verginia Polytechnic Institute and State University, Ph.D. thesis.
3. Garcia, F.R. (1983), "Mathematical Modelling of Two-Dimentional Hydraulic Problems Using a Fully-Dense Finite-Difference Scheme", M.Sc.A. Thesis, Ecole Polytechnique de Montreal, August.
4. Hewlett, Y. B. (1976), "Rate of Recession of The Leading Edge of Ice Covers on Open Channel Flows", University of Iowa, Masters Thesis.
5. McGuirk,J.J., and Rodi,W. (1978), "A Depth-Averaged Mathematical Model for The Near Field of Side Discharges Into Open-channel Flow", Journal of Fluid Mechanics, Vol.86, Part 4, pp.761-781.
6. Saadé, R. (1990), "Numerical Modelling of Ice Cover Melting Under Turbulent Flow Conditions", M.A.Sc. Thesis, Concordia University, December.
7. Shen, T.S., and Chiang, L. (1984), "Simulation of Growth and Decay of River Ice Cover", Journal of Hydraulic Engineering, ASCE, Vol. 110, No. 7, July, pp. 958-971.

LIST OF SYMBOLS

C_c = coefficient used in conductive heat transfer

C_e = coefficient used in evapo-condensation heat flux

C_{wi} = heat transfer constant water to ice, in cal $s^{-0.2}$ $m^{-2.6}$ $°C^{-1}$

e_a = air vapour pressure, in mb

e_s = saturation vapour pressure, in mb

n = Combined Manning's coefficient

n_b = Manning's coefficient of river bed

n_i = Manning's coefficient of the underside of ice cover

q_{wi} = heat flux, water to ice cover, in cal $m^{-2}s^{-1}$

V_a = wind velocity at 2 m above surface, in m s^{-1}

α = surface albedo

ε_s = emissivity of water or ice surface

θ	=	ice cover thickness, in m
τ_i	=	bulk extinction coefficient, in cm^{-1}
ϕ_b	=	effective back radiation, in cal cm^{-2} day^{-1}
ϕ_{ba}	=	atmospheric radiation, in cal cm^{-2} day^{-1}
ϕ_{bn}	=	net atmospheric radiation, in cal cm^{-2} day^{-1}
ϕ_{bs}	=	longwave radiation emitted by the river surface
ϕ_c	=	conductive heat transfer, in cal cm^{-2} day^{-1}
ϕ_e	=	evapo-condensation flux, in cal $cm^{-2}day^{-1}$
ϕ_{lat}	=	latitude on earth's surface, in degrees
ϕ_{ri}	=	incoming shortwave radiation, in cal cm^{-2} day^{-1}
ϕ_s	=	net shortwave radiation, in cal cm^{-2} day^{-1}
ϕ_{sp}	=	shortwave penetration into the waterbody, in cal cm^{-2} day^{-1}